Ab initio multiconfiguration Dirac-Hartree-Fock calculations of the In and Tl electron affinities and their isotope shifts

Ran Si,[1,2] Sacha Schiffmann,[2,3] Kai Wang,[4] Chong Yang Chen,[1,*] and Michel Godefroid[2,†]

[1]*Shanghai EBIT Lab, Key Laboratory of Nuclear Physics and Ion-beam Application, Institute of Modern Physics, Department of Nuclear Science and Technology, Fudan University, Shanghai 200433, People's Republic of China*

[2]*Spectroscopy, Quantum Chemistry and Atmospheric Remote Sensing (SQUARES), CP160/09, Université libre de Bruxelles, 1050 Brussels, Belgium*

[3]*Division of Mathematical Physics, Department of Physics, Lund University, Box 118, SE-22100 Lund, Sweden*

[4]*Hebei Key Lab of Optic-electronic Information and Materials, The College of Physics Science and Technology, Hebei University, Baoding 071002, People's Republic of China*

(Received 22 February 2021; revised 18 May 2021; accepted 21 June 2021; published 7 July 2021)

We report multiconfiguration Dirac-Hartree-Fock and relativistic configuration interaction calculations on the thallium (Tl) electron affinity, as well as on the excited energy levels arising from the ground configuration of Tl^-. The results are compared with the available experimental values and further validated by extending the study to its homologous, lighter element, indium (In), belonging to group 13 (III.A) of the Periodic Table. The calculated electron affinities of In and Tl, 383.4 and 322.8 meV, agree with the latest measurements by within 1%. Three bound states $^3P_{0,1,2}$ are confirmed in the $5s^25p^2$ configuration of In^-, while only the ground state $^3P_0$ is bound in the $6s^26p^2$ configuration of Tl^-. The isotope shifts on the In and Tl electron affinities are also estimated. The E2 and M1 intraconfiguration radiative transition rates within $5s^25p^2\ ^3P_{0,1,2}$ of In^- are used to calculate the radiative lifetimes of the metastable $^3P_{1,2}$ levels.

DOI: 10.1103/PhysRevA.104.012802

I. INTRODUCTION

Negative ions play a major role in a number of areas of physics and chemistry involving ionized gases and plasma. Since there is no long-range Coulomb interaction between the outermost electron and the atomic core, their properties critically depend on electron-electron correlation and polarization, and negative ions will only have a few bound states, if any. In most cases, the latter have the same parity or even belong to the same electronic configuration. Only in a few cases, namely Os^- [1–3], Ce^- [4,5], La^- [6–8], and Th^- [9,10], do negative ions have excited bound states of opposite parity to that of the ground state, making them good candidates for laser cooling. The most promising ones so far are La^- and Th^-.

Several experimental techniques are possible to measure atomic electron affinities (EAs) and excited energy levels of negative ions with high precision. Nevertheless, some atomic electron affinities and anion fine-structure splittings are still known with limited accuracy. All elements of group 13 (B, Al, Ga, In, and Tl) form stable negative ions with electron affinities of less than 0.5 eV. The latter are therefore challenging to determine with accuracy, especially for the heavier elements. Recently, tunable laser photodetachment threshold spectroscopy (LPTS) was used to measure the electron affinity of the $6s^26p^2\ ^3P_0$ ground state of $^{205}Tl^-$ to be 320.053(19) meV [11], which differs significantly from the value of 377(13) meV obtained by a fixed-frequency laser photodetachment electron spectroscopy (LPES) measurement [12]. Both experiments indicate that the excited levels are either unbound or too weakly bound to be detected, although the three fine-structure levels $^3P_{0,1,2}$ were detected as bound states for the lighter elements of the same group 13 (B^-, Al^-, Ga^-, and In^-) [13–18]. A number of theoretical studies on the EA of Tl have been reported using a variety of computational methods [19–26], but their results show poor agreement. For example, using different theoretical methods, Arnau *et al.* [19] and Felfli *et al.* [25] predicted the EA of Tl to be 270 and 2415 meV, respectively.

In the present study, we resolve the disagreement between experimental and theoretical EA values of Tl, and we explore the existence of bound excited states of Tl^-. Since the ground configurations of In ($5s^25p$) and In^- ($5s^25p^2$) are analogous to those of Tl ($6s^26p$) and Tl^- ($6s^26p^2$), we use the In/In^- system as a benchmark to support our Tl/Tl^- analysis. We also estimate the balance between the nuclear mass and volume contributions to the isotope shift (IS) on electron affinities of different isotopes of In and Tl. The radiative lifetimes of the excited In^- $5s^25p^2\ ^3P_{1,2}$ fine-structure levels based on the intraconfiguration radiative decay rates are reported.

II. THEORY

A. Multiconfiguration Dirac-Hartree-Fock approach

The multiconfiguration Dirac-Hartree-Fock (MCDHF) method [27], as implemented in the GRASP computer package

*chychen@fudan.edu.cn
†Michel.Godefroid@ulb.be

[28,29], is employed to obtain wave functions that are referred to as atomic state functions (ASFs), i.e., approximate eigenfunctions of the Dirac-Coulomb Hamiltonian given by

$$H_{\rm DC} = \sum_{i=1}^{N}[c\,\boldsymbol{\alpha_i}\cdot\boldsymbol{p_i} + (\beta_i - 1)c^2 + V_i] + \sum_{i<j}^{N}\frac{1}{r_{ij}}, \quad (1)$$

where V_i is the monopole part of the electron-nucleus interaction for a finite nucleus, r_{ij} is the distance between electrons i and j, and $\boldsymbol{\alpha}$ and β are the Dirac matrices.

Electron correlation is included by expanding $\Psi(\gamma PJ)$, an ASF, over a linear combination of configuration state functions (CSFs) $\Phi(\gamma_i PJ)$,

$$\Psi(\gamma PJ) = \sum_{i=1}^{M} c_i \Phi(\gamma_i PJ), \quad (2)$$

where γ_i represents all the coupling tree quantum numbers needed to uniquely define the CSF, besides the parity P and the total angular momentum J. The CSFs are spin-angular coupled antisymmetric products of four-component Dirac orbitals of the form

$$\phi(\mathbf{r}) = \frac{1}{r}\begin{pmatrix} P_{n\kappa}(r)\chi_{\kappa m}(\theta,\phi) \\ iQ_{n\kappa}(r)\chi_{-\kappa m}(\theta,\phi)\end{pmatrix}. \quad (3)$$

The radial parts of the one-electron orbitals and the expansion coefficients c_i of the CSFs are obtained by the relativistic self-consistent-field (RSCF) procedure. In the present paper, the CSF expansions are obtained using the restricted active set (RAS) method by allowing single and double (SD) substitutions from a selected set of reference configurations to a given orbital active set. The latter is systematically expanded by the addition of successive orbital layers to monitor the convergence of the calculated energies or any other relevant observable. To efficiently capture the required variational flexibility and describe appropriately the electronic redistribution accompanying the detachment, the mixing coefficients and orbitals are optimized separately for the targeted states of the anion and the neutral atom.

Each RSCF calculation is followed by a relativistic configuration interaction (RCI) calculation, where the Dirac orbitals are kept fixed and only the expansion coefficients of the CSFs are determined for selected eigenvalues and eigenvectors of the complete interaction matrix. In this procedure, the Breit interaction and leading quantum electrodynamic (QED) effects (vacuum polarization and self-energy) are included.

In addition to energy levels, lifetimes τ and transition parameters, such as transition rates A and line strengths S, are also computed. The transition parameters between two states $\gamma' P' J'$ and γPJ are expressed in terms of reduced matrix elements of the relevant transition operators [30,31]:

$$\langle\Psi(\gamma PJ)||\mathbf{T}||\Psi(\gamma' P' J')\rangle = \sum_{k,l} c_k c_l' \langle\Phi(\gamma_k PJ)||\mathbf{T}||\Phi(\gamma_l' P' J')\rangle. \quad (4)$$

Biorthogonal orbital transformations and CSF-expansion counter-transformations are used [32] when radial nonorthogonalities arise from the independent optimization of the two ASFs involved in (4).

B. Isotope shift

We define the isotope shift (IS) on the EA between two isotopes of mass A and A' as

$$\mathrm{IS(EA)}^{AA'} = \mathrm{EA}(A) - \mathrm{EA}(A'), \quad (5)$$

in agreement with the frequency isotope shift definition adopted in the description of the RIS3 [33] and RIS4 [34] codes. In the $A > A'$ case, a positive isotope shift on the EA implies a larger electron affinity for the heavier isotope. Such an IS is qualified as a "normal" IS, referring to the normal mass shift encountered for the one-electron atomic hydrogen characterized by a blueshift of the spectral lines of deuterium ^{2}H compared with hydrogen ^{1}H. The IS can be decomposed into two contributions: the mass shift (MS) and the field shift (FS). They arise, respectively, from the recoil effect due to the finite mass of the nucleus, and from the difference in nuclear charge distributions between the two isotopes. The revised version of the RIS3 code [33], RIS4 [34], is used for the computations of IS parameters in the present paper. The nuclear recoil corrections within the Breit approximation are considered in these two codes, together with a reformulation of the field shift in RIS4. Although QED corrections to the MS parameters were studied recently by other authors [35–37] in few-electron atoms, these elaborate developments are beyond the scope of the present work and could be considered in the future.

1. Mass shift

The isotope mass shift of an atomic level i is obtained by evaluating the expectation values of the operator,

$$H_{\rm MS} = \frac{1}{2M}\sum_{j,k}^{N}\left[\boldsymbol{p}_j\cdot\boldsymbol{p}_k - \frac{\alpha Z}{r_j}\left(\boldsymbol{\alpha}_j + \frac{(\boldsymbol{\alpha}_j\cdot\boldsymbol{r}_j)\boldsymbol{r}_j}{r_j^2}\right)\cdot\boldsymbol{p}_k\right], \quad (6)$$

where M is the nuclear mass of the isotope [38].

Separating the operator into one-body and two-body terms, $H_{\rm MS}$ can be rewritten as the sum of normal mass shift (NMS) and specific mass shift (SMS) contributions,

$$H_{\rm MS} = H_{\rm NMS} + H_{\rm SMS}. \quad (7)$$

The (mass-independent) normal mass shift $K_{\rm NMS}$ and specific mass shift $K_{\rm SMS}$ parameters for a level i are defined by the following expressions:

$$\frac{K_{i,\rm NMS}}{M} \equiv \langle\Psi_i(\gamma PJ)|H_{\rm NMS}|\Psi_i(\gamma PJ)\rangle, \quad (8)$$

$$\frac{K_{i,\rm SMS}}{M} \equiv \langle\Psi_i(\gamma PJ)|H_{\rm SMS}|\Psi_i(\gamma PJ)\rangle. \quad (9)$$

The mass shift parameters can be decomposed into three parts,

$$K_{i,\rm NMS} = K^1_{i,\rm NMS} + K^2_{i,\rm NMS} + K^3_{i,\rm NMS}, \quad (10)$$

$$K_{i,\rm SMS} = K^1_{i,\rm SMS} + K^2_{i,\rm SMS} + K^3_{i,\rm SMS}, \quad (11)$$

where the K^1 terms refer to the "uncorrected" relativistic contributions [first term of (6)] and the sum $K^2 + K^3$ [second and third terms of (6)] to the lowest-order relativistic corrections in the Breit approximation [39–42].

The mass shift contribution to the IS on the EA,

$$\mathrm{IS(EA)}^{AA'}_{\mathrm{MS}} = \Delta K_{\mathrm{MS}}\left(\frac{1}{M} - \frac{1}{M'}\right), \tag{12}$$

is therefore directly proportional to the difference of the MS electronic parameters

$$\Delta K_{\mathrm{MS}} = K_{\mathrm{g.s.,MS}} - K^{-}_{\mathrm{g.s.,MS}}, \tag{13}$$

where the minus exponent refers to quantities related to the negative ion, and g.s. stands for ground state.

2. Field shift

In the first-order perturbation approximation, the field shift for a given level i can be expressed as

$$\delta E^{(1)A,A'}_{i,\mathrm{FS}} = -\int_{\boldsymbol{R^3}} [V^{A}(\boldsymbol{r}) - V^{A'}(\boldsymbol{r})]\rho^{e}_{i}(\boldsymbol{r})d^3\boldsymbol{r}, \tag{14}$$

where $V^{A}(\boldsymbol{r})$ and $V^{A'}(\boldsymbol{r})$ are the potentials arising from the nuclear charge distributions of the two isotopes, and $\rho^{e}_{i}(\boldsymbol{r})$ is the electron density. By approximating the electron density at the origin with a spherically symmetric even polynomial function

$$\rho^{e}_{i}(\boldsymbol{r}) \approx b_{i,0} + b_{i,2}r^2 + b_{i,4}r^4 + b_{i,6}r^6, \tag{15}$$

Eq. (14) can be expressed as

$$\delta E^{(1)A,A'}_{i,\mathrm{FS}} \approx \sum_{0\leqslant n\leqslant 6,\mathrm{even}} F_{i,n}\ \delta\langle r^{n+2}\rangle^{A,A'}, \tag{16}$$

where $F_{i,n}$ are level electronic factors and $\delta\langle r^n\rangle^{A,A'} = \langle r^n\rangle^{A} - \langle r^n\rangle^{A'}$. Assuming a constant electron density within the nuclear volume, we get from the first term of Eq. (16),

$$\delta E^{(1)A,A'}_{i,\mathrm{FS}} \approx F_{i,0}\ \delta\langle r^2\rangle^{A,A'}. \tag{17}$$

As suggested in Refs. [34,43], we can include the effect of a varying electronic density (ved) to evaluate the FS by introducing the appropriate corrected level electronic factors, $F^{(0)\mathrm{ved}}_{i,0}$ and $F^{(1)\mathrm{ved}}_{i,0}$, without considering higher-order nuclear moments. Equation (16) is then replaced by

$$\delta E^{(1)A,A'}_{i,\mathrm{FS}} \approx \left(F^{(0)\mathrm{ved}}_{i,0} + F^{(1)\mathrm{ved}}_{i,0}\delta\langle r^2\rangle^{A,A'}\right)\delta\langle r^2\rangle^{A,A'}. \tag{18}$$

The FS contribution to the IS on the EA can therefore be estimated from

$$\mathrm{IS(EA)}^{AA'}_{\mathrm{FS}} = (F_{\mathrm{g.s.},0} - F^{-}_{\mathrm{g.s.},0})\delta\langle r^2\rangle^{A,A'} \tag{19}$$

with

$$(F_{\mathrm{g.s.},0} - F^{-}_{\mathrm{g.s.},0}) = \Delta F_0 \tag{20}$$

in the constant electron density approximation, or

$$(F_{\mathrm{g.s.},0} - F^{-}_{\mathrm{g.s.},0}) = \left(\Delta F^{(0)\mathrm{ved}}_{0} + \Delta F^{(1)\mathrm{ved}}_{0}\delta\langle r^2\rangle^{A,A'}\right) \tag{21}$$

using the varying electronic density model.

III. RESULTS AND DISCUSSIONS

A. Electron affinities

To evaluate the ground-state energies of the Tl neutral atom ($[\mathrm{Xe}]4f^{14}5d^{10}6s^26p\ \ ^2P^o_{1/2}$) and Tl^- anion ($[\mathrm{Xe}]4f^{14}5d^{10}6s^26p^2\ \ ^3P_0$), we start from single-reference (SR) calculations, where CSF lists are generated by allowing single and double (SD) excitations from the $5d$, $6s$, and $6p$ electrons to orbitals with $n \leqslant 10$, $l \leqslant 5$. The CSFs that contribute by more than 0.1% in weight ($w_i = |c_i|^2$) to the ground-state wave functions of Tl and Tl^- are reported in Table I. The EA value obtained from these SD-SR calculations is around 118 meV, a result that greatly underestimates the LPTS [11] and LPES [12] experimental values of 320.053(19) and 377(13) meV, respectively. The single- and double-multireference (SD-MR) method is then employed to better balance the neutral atom and anion. The configurations

$$\begin{aligned}\mathrm{Tl\ (odd)} &: 5d^{10}6s^26p,\ 5d^85f^26s^26p,\ 5d^{10}6p^3,\\ \mathrm{Tl^-\ (even)} &: 5d^{10}6s^26p^2,\ 5d^85f^26s^26p^2,\\ &\quad 5d^{10}6p^4,\ 5d^{10}6s6p^26d,\ 5d^95f6s6p^27p,\end{aligned} \tag{22}$$

selected on the basis of the wave-function compositions of Table I, form the multireference (MR) spaces used in the following. When adopting the SD-MR process for generating the CSF expansions, higher-order excitations such as triple and quadruple (TQ) excitations from the single-reference are naturally captured.

In the MR calculations, SD excitations are allowed from all MR configurations to an increasingly active set (AS) of orbitals. The calculations are performed layer by layer, introducing at each step at most one new correlation orbital per angular κ-symmetry. Excitations from the SR configuration are ultimately allowed to an active set of orbitals with $n \leqslant 13$ and $l \leqslant 5$, denoted $13h$. Excitations from the remaining MR configurations are, however, limited to smaller active sets, i.e., $6s6p6d5f$ for the neutral atom and $8s8p7d6f$ for the anion, to keep the number of CSFs manageable. The slightly larger active set for the anion is required to balance correlation effects between the atom and its anion. Two sets of calculated EAs with increasing ASs are listed in Table II. One is $\mathrm{EA}(\Delta n = 0) = E_n(\mathrm{Tl}) - E_n(\mathrm{Tl}^-)$, where E_n labels the energy obtained with the AS of maximum principal quantum number n, the other is $\mathrm{EA}(\Delta = 1) = E_n(\mathrm{Tl}) - E_{n+1}(\mathrm{Tl}^-)$, which can be justified by the fact that more orbitals are needed to describe electron correlation for the negative ion than for the neutral atom. The former is increasing with active sets and provides a lower bound to the calculated EA, whereas the latter is decreasing and hence provides an upper bound. We used a nonlinear exponential decay function to extrapolate the last four $\mathrm{EA}(\Delta n = 0)$ and $\mathrm{EA}(\Delta n = 1)$ values, and we adopted the intersection as our final theoretical EA value [44]. The theoretical uncertainty of the *ab initio* EA inevitably depends on the correlation models used for tailoring the ASF expansions. Based on our past experience on complex systems [9,44], on the analysis of the convergences over n and l values (which are around 1% and 1.5%, respectively), and on the comparison with observation [9,45], we estimated the theoretical uncertainty to be less than 2%. This conservative estimation covers the 0.8% corresponding to half of the interval between the two $\mathrm{EA}(\Delta n = 0, 1)$ values and the smaller uncertainty (0.65%) associated with the extrapolation procedure. With this uncertainty estimation, our final thallium EA-value is 322.8(6.5) meV.

TABLE I. Wave-function compositions for the ground states of Tl and Tl^-. See the text for the definition of the weights w_i.

Tl			Tl^-		
Configuration	Term	w_i(%)	Configuration	Term	w_i(%)
$5d^{10}6s^26p$	$^2P^o$	92.1	$5d^{10}6s^26p^2$	^3P	81.9
$5d^8(^3P)5f^2(^1S)6s^26p$	$^2P^o$	0.61	$5d^{10}6s^26p^2$	^1S	8.84
$5d^8(^3F)5f^2(^1S)6s^26p$	$^2P^o$	0.53	$5d^8(^3P)5f^2(^1S)6s^26p^2$	^3P	0.55
$5d^{10}6p^3$	$^2P^o$	0.47	$5d^8(^3F)5f^2(^1S)6s^26p^2$	^3P	0.48
$5d^8(^1D)5f^2(^1S)6s^26p$	$^2P^o$	0.25	$5d^8(^1D)5f^2(^1S)6s^26p^2$	^3P	0.22
$5d^8(^1S)5f^2(^1S)6s^26p$	$^2P^o$	0.15	$5d^{10}6p^4$	^3P	0.18
$5d^8(^1G)5f^2(^1S)6s^26p$	$^2P^o$	0.14	$5d^8(^1S)5f^2(^1S)6s^26p^2$	^3P	0.13
			$5d^8(^1G)5f^2(^1S)6s^26p^2$	^3P	0.12
			$5d^{10}6s6p^2(^2D)6d$	^3P	0.12
			$5d^95f(^1P)6s(^2P^o)6p^2(^4D)7p$	^3P	0.11
			$5d^95f(^1P)6s(^2P^o)6p^2(^2D)7p$	^3P	0.10
			$5d^95f(^1P)6s(^2P^o)6p^2(^4P)7p$	^3P	0.10

A comparison between experimental and theoretical EA values is presented in Table III. One can see that our final thallium EA-value of 322.8(6.5) meV agrees with the very recent LPTS experimental value of 320.053(19) meV [11], but definitely lies outside the error bars of the previous LPES measurement 377(13) meV [12]. As mentioned in the introduction, the scattering of theoretical results is surprisingly large. Among the most recent works, our MCDHF-RCI value is in good agreement with the results of Finneyet *et al.* [26] using the relativistic coupled-cluster version of the Feller-Peterson-Dixon composite method (RCC-FPD). Our theoretical estimation is definitely smaller—by almost one order of magnitude—than the complex angular momentum (CAM) electron elastic total cross-sections result of Felfli *et al.* [25]. The latter authors suggested that all the EA values of thallium reported in the literature before their work should be considered as the binding energy of an excited state of the anion. All RCI calculations performed in the present work for the odd parity exclude this possibility, the lowest state, $5d^{10}6s6p^3\ ^5S^o_2$, being estimated to lie around 5.2 eV above the ground level of Tl^-.

Since In and $In^-(Z = 49)$ are homologous elements to Tl and Tl^- $(Z = 81)$, we performed similar calculations for the electron affinity of In to further validate our calculated EA of thallium. SD excitations from $4d^{10}5s^25p$ and $4d^{10}5s^25p^2$ are allowed up to orbitals with $n \leqslant 12$, $l \leqslant 5$; SD excitations from $4d^84f^25s^25p$ and $4d^{10}5p^3$ are allowed up to the $5s5p5d4f$ AS for the In neutral atom; SD excitations from $4d^84f^25s^25p^2$, $4d^{10}5p^4$, $4d^{10}5s5p^25d$, and $4d^95f^25s5p^26p$ are included up to the $7s7p6d5f$ AS for the In^- anion. The calculated EA($\Delta n = 0$) and EA($\Delta n = 1$) values are also listed in Table II. Using the same extrapolation method as for Tl^-, we obtain a final value of 383.4(7.7) meV for which we adopted the 2% uncertainty estimation, as discussed above, that largely covers half of the interval between the two EA($\Delta n = 0, 1$) values (1.1%). This theoretical result is also in excellent agreement with the LPTS experimental value of 383.92(6) meV [18]. Similarly as for thallium, our indium EA value lies outside the confidence interval of the LPES measurement of 404(9) meV [13].

TABLE II. Theoretical electron affinities of In and Tl (present work). All values in meV.

In			Tl		
AS	EA($\Delta n = 0$)	EA($\Delta n = 1$)	AS	EA($\Delta n = 0$)	EA($\Delta n = 1$)
9h	356.2	428.6	10h	303.3	342.1
10h	368.5	398.6	11h	311.9	327.9
11h	374.4	390.0	12h	315.9	324.7
12h	378.1	386.5	13h	318.5	323.7
Final	383.4(7.7)			322.8(6.5)	

TABLE III. Comparison of the present calculated electron affinities of In and Tl with the experimental results and other theoretical values. LPTS: laser photoelectron threshold spectroscopy, LPES: laser photodetachment electron spectroscopy, MCDHF: multiconfiguration Dirac-Hartree-Fock calculations (present work), CIPSI: multireference single and double configuration-interaction method, RCC: relativistic coupled cluster, HFR-DFT: pseudorelativistic Hartree-Fock and density functional theory, IHFSCC: intermediate-Hamiltonian Fock-space coupled cluster method, CAM: complex angular momentum method, RCC-FPD: relativistic coupled-cluster version of the Feller-Peterson-Dixon composite method. (All values in meV).

	Method	EA(In)	EA(Tl)
	Experiment		
Walter *et al.* [18]	LPTS	383.92(6)	
Walter *et al.* [11]	LPTS		320.053(19)
Williams *et al.* [13]	LPES	404(9)	
Carpenter *et al.* [12]	LPES		377(13)
	Theory		
Present work	MCDHF	383.4(7.7)	322.8(6.5)
Wijesundera [20]	MCDHF	393	291
Li *et al.* [24]	MCDHF	397.83	290.20
Arnau *et al.* [19]	CIPSI	380	270
Eliav *et al.* [21]	RCC	419	400
Chen and Ong [22]	HFR-DFT	429	388
Figgen *et al.* [23]	IHFSCC	403	347
Felfli *et al.* [25]	CAM	380	2415
Finney *et al.* [26]	RCC-FPD	386	320

TABLE IV. Isotope shift parameters on the electron affinities of In and Tl. ΔK values in GHz*u. ΔF_0 and ΔF_0^{ved} in GHz/fm^2, $\Delta F_0^{(1)\text{ved}}$ in GHz/fm^4.

	In/In$^-$	Tl/Tl$^-$
ΔK^1_{NMS}	−134	−74
$\Delta\left(K^2_{\text{NMS}} + K^3_{\text{NMS}}\right)$	−65	−194
ΔK_{NMS}	−199	−268
ΔK^1_{SMS}	41	68
$\Delta\left(K^2_{\text{SMS}} + K^3_{\text{SMS}}\right)$	−34	−245
ΔK_{SMS}	6	−178
$\Delta K_{\text{MS}} = \Delta K_{\text{NMS}} + \Delta K_{\text{SMS}}$	−192	−445
ΔF_0	0.814	7.21
$\Delta F_0^{(0)\text{ved}}$	0.791	6.68
$\Delta F_0^{(1)\text{ved}}$	4.47×10^{-4}	7.11×10^{-3}

B. Isotope shifts on the indium and thallium electron affinities

Both In and Tl have many isotopes. While the stable isotope ^{113}In is only 4.3% of naturally occurring indium, in lower abundance than the long-lived radioactive isotopes, Tl has two stable isotopes, ^{203}Tl (30% natural abundance) and ^{205}Tl (70%). In this section, we report the isotope shifts on the electron affinity of In and Tl by using the wave functions obtained for estimating the electron affinity (see the previous section). The differences of the isotope shift mass and field electronic parameters that make the IS on the EA [see Eqs. (13) and (19)] are listed in Table IV.

From this table, we can see that for In, the sum of the relativistic corrections to the uncorrected one-electron normal mass shift operator, $\Delta(K^2_{\text{NMS}} + K^3_{\text{NMS}})$, reinforces the ΔK^1_{NMS} value by around 50%, while for the SMS, $\Delta(K^2_{\text{SMS}} + K^3_{\text{SMS}})$ counterbalances ΔK^1_{SMS} by 85%, leading to a large dominance of ΔK_{NMS} over ΔK_{SMS}.

Relativistic corrections to the recoil operator play an even more important role in Tl, for which $\Delta(K^2_{\text{NMS}} + K^3_{\text{NMS}})$ is 2.6 times larger than the uncorrected ΔK^1_{NMS} value, and they strongly strengthen it. For the SMS contribution, the $\Delta(K^2_{\text{SMS}} + K^3_{\text{SMS}})$ is 3.6 times larger than ΔK^1_{SMS} but of opposite sign. Opposite to In, the total ΔK_{SMS} value is large, 66% of the ΔK_{NMS}, and the constructive addition of both contributions makes the total ΔK_{MS} value 1.66 times larger than the NMS contribution.

The differences of the electronic FS parameters are reported in Table IV for both In/In$^-$ and Tl/Tl$^-$ systems. Positive ΔF values reveal a gain in electron density at the nucleus when detaching the outer electron from the anion. One should observe that this gain factor is 10 times larger for thallium than for indium. The ratio of the Tl and In nuclear charges $Z(\text{Tl})/Z(\text{In}) \approx 1.65$, arising from the explicit linear Z-dependence of the FS factor [33,34], can only explain a small portion of this difference. The much larger remaining part of this factor 10 is simply due to the Tl-In difference of the electron density within the nuclear volume. The FS contribution to the IS on the EA has been estimated from Eqs. (19) and (21) to include the effect of a varying electronic density, using the root mean square (rms) nuclear radii from Ref. [46].

TABLE V. Mass (MS), field (FS), and total (MS+FS) isotope shifts on EAs relative to the most abundant isotopes, i.e., EA(^{A}In)-EA(^{113}In) and EA(^{A}Tl)-EA(^{205}Th). All shifts in GHz.

	In				Tl		
A	MS	FS	MS+FS	A	MS	FS	MS+FS
104	−0.147	−0.596	−0.744	188	−0.197	−5.397	−5.594
105	−0.130	−0.505	−0.635	190	−0.172	−4.645	−4.816
106	−0.113	−0.459	−0.572	191	−0.159	−4.297	−4.456
107	−0.096	−0.374	−0.469	192	−0.147	−4.137	−4.285
108	−0.079	−0.318	−0.397	193	−0.135	−3.760	−3.895
109	−0.063	−0.236	−0.298	194	−0.123	−3.644	−3.767
110	−0.047	−0.195	−0.241	195	−0.112	−3.165	−3.276
111	−0.031	−0.112	−0.143	196	−0.100	−3.150	−3.250
112	−0.015	−0.075	−0.090	197	−0.088	−2.707	−2.795
113	**0.000**	**0.000**	**0.000**	198	−0.077	−2.649	−2.725
114	0.015	0.034	0.048	199	−0.066	−2.044	−2.110
115	0.030	0.106	0.136	200	−0.054	−1.957	−2.011
116	0.044	0.147	0.191	201	−0.043	−1.359	−1.402
117	0.058	0.206	0.264	202	−0.032	−1.198	−1.231
118	0.072	0.237	0.310	203	−0.021	−0.680	−0.701
119	0.086	0.290	0.376	204	−0.011	−0.402	−0.413
120	0.100	0.317	0.416	**205**	**0.000**	**0.000**	**0.000**
121	0.113	0.362	0.475	207	0.021	0.688	0.709
122	0.126	0.384	0.510	208	0.031	1.370	1.402
123	0.139	0.428	0.567				
124	0.152	0.451	0.602				
125	0.164	0.484	0.648				
126	0.176	0.507	0.684				
127	0.188	0.530	0.719				

The mass, field and total isotope shifts on electron affinities are reported in Table V and displayed in Fig. 1 for a large range of isotopes relative to the ^{113}In and ^{205}Tl stable isotopes.

We observe that for EA(In), the FS is already more important than the MS, while for EA(Tl), the FS largely dominates the MS that becomes almost negligible. This is expected for heavy elements, as the mass factor $1/M - 1/M' = (M' - M)/MM'$ decreases rapidly with the nuclear mass. For example, the MS contribution to the electron affinities between the two stable isotopes of Tl, ^{203}Tl and ^{205}Tl, is $\text{IS(EA)}^{205,203}_{\text{MS}} = 0.0214$ GHz. If we assume a constant electron density within the nuclear volume, Eq. (17) gives a FS of $\text{IS(EA)}^{205,203}_{\text{FS}} = 0.7334$ GHz. By including the effect of a varying electronic density, Eq. (18) gives a FS of 0.6799 GHz, which is 7% lower than the former value. This observation is consistent with previous studies on IS (see, e.g., [34,47]) and emphasizes the need to include this effect. Adding the MS and latter FS contributions together, we obtain that EA(^{205}Tl) is 0.7014 GHz higher than EA(^{203}Tl), i.e., $\text{IS(EA)}^{205,203} = 0.7014$ GHz.

C. ns^2np^2 levels of In$^-$ ($n = 5$) and Tl$^-$ ($n = 6$)

The RCI excitation energies of the four levels $5s^25p^2\ ^3P_{1,2}$, $^1D_2$, and $^1S_0$ of In$^-$ based on the wave functions described in Sec. III B are reported in Table VI. The In$^-$ energy levels relative to the ground state of In ($5s^25p\ ^2P^o_{1/2}$) are also displayed in Fig. 2(a).

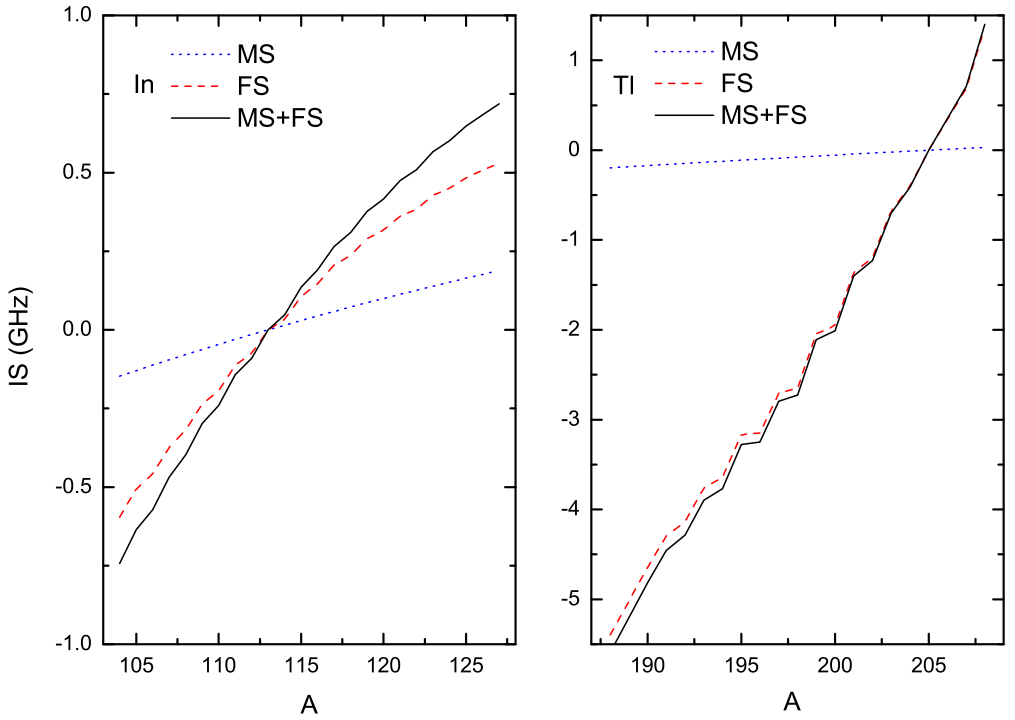

FIG. 1. Mass (MS), field (FS), and total (MS+FS) isotope shifts (IS) on EAs relative to ^{113}In and ^{205}Th, i.e., EA(^{A}In)-EA(^{113}In) and EA(^{A}Tl)-EA(^{205}Th).

The excited energy levels $5s^25p^2\ ^3P_1$ and $^3P_2$ of In^- have been observed as being stable using the techniques of laser-photodetachment electron spectroscopy (LPES) [13] and laser-photodetachment threshold spectroscopy (LPTS) [18]. Our theoretical work confirms the existence of three bound states in In^-, all belonging to the ^3P fine structure. The theory-observation agreement is quite satisfactory. The presently calculated $^3P_1$ energy level agrees within 0.6 meV with the two experimental values, while the $^3P_2$ energy level is predicted to be 9 meV higher than the result of the LPTS measurement [13].

Similar RCI calculations were performed for the energy levels $6s^26p^2\ ^3P_{1,2}$, $^1D_2$, and $^1S_0$ of Tl^-. The corresponding excitation energies are displayed relative to the Tl ground state ($6s^26p\ ^2P^o_{1/2}$) in Fig. 2(b). We can see that due to the large fine-structure splitting of $6s^26p^2\ ^3P_{0,1,2}$, the $^3P_0$ level is the only bound state in Tl^-, which agrees with the interpretation of the recent threshold spectroscopy measurements [11].

TABLE VI. Excitation energies (in meV) and radiative lifetimes (τ, in s) of the In^- $5s^25p^2\ ^3P_{1,2}$ levels. MCDHF: present work, LPTS: laser photoelectron threshold spectroscopy measurements [18], LPES: laser photodetachment electron spectroscopy [13], MCDHF (adj.): adjusted lifetimes using the LPTS experimental transition energies [18].

	Excitation energies (meV)			τ (s)	
	MCDHF	LPTS	LPES	MCDHF	MCDHF (adj.)
$^3P_1$	75.43	76.06(7)	76(9)	251.8	245.6
$^3P_2$	179.4	170.6(6)	175(9)	129.8	172.7

The $^1D_2$ and $^1S_0$ levels are both unbound in In^- and Tl^- (see Fig. 2). For both systems, the $^1D_2$ level of the anion and the $^2P^o_{3/2}$ level of the corresponding neutral atom are almost degenerate.

Recent progress has been made in the measurements of radiative lifetimes of metastable levels of negative ions using cold storage techniques [48,49]. It is therefore worthwhile to report the theoretical lifetimes of the In^- $5s^25p^2\ ^3P_{1,2}$ levels that have not been measured yet so far. Our predicted lifetimes, based on our theoretical M1 and E2 radiative decay rates, are reported in Table VI. Looking at the selection rules [31], the $^3P_1$ level can only decay to the ground state $^3P_0$ through a magnetic dipole (M1) process. The $^3P_2$ level can decay to $^3P_0$ via an electric quadrupole (E2) radiative transition, and to $^3P_1$ through both M1 and E2 deexcitations, but the E2 transition probabilities are found to be much smaller than the M1 amplitudes by at least two to three orders of magnitude. This means that the theoretical lifetimes mostly depend on the M1 rates that usually quickly converge with the correlation models [50]. The quality of the transition energies is, however, an important ingredient due to the λ^3 scaling factor appearing in the M1 spontaneous emission A rate. For this reason, we also report the adjusted lifetimes to the experimental excitation energies [51], measured in the LPTS [18] experiment. The resulting lifetimes of a few hundred seconds could be measured in a cryogenic ion storage ring that was demonstrated to be efficient to store negative ion beams in the hour time domain [48,49].

IV. CONCLUSION

In summary, we calculated the EAs of In and Tl to be 383.4 and 322.8 meV, respectively. These results agree with the

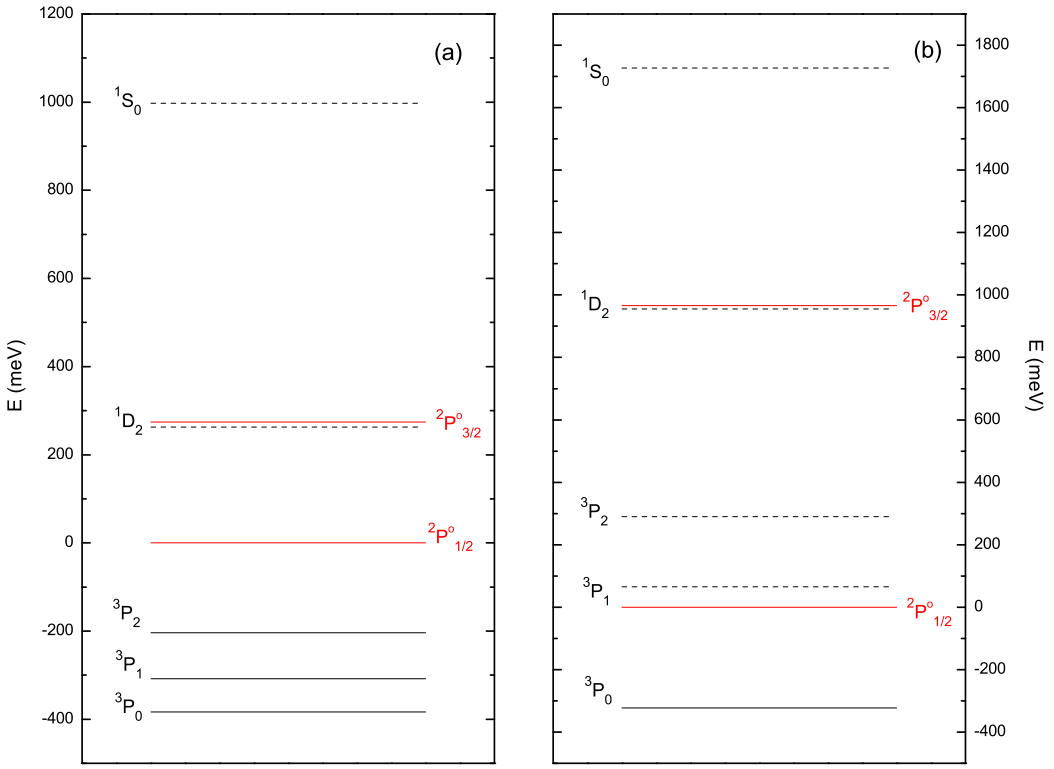

FIG. 2. Energy diagram of $5s^25p^2$ levels of In^- (a) and $6s^26p^2$ levels of Tl^- (b) relative to the ground states of In and Tl, respectively. The fine-structure splitting of $^2P^o_{1/2,3/2}$ for the neutral atoms are from NIST ASD [52].

latest LPTS experimental measurements [11,18] within 1%. The significant disagreement between the present theoretical EAs and the (too large) LPES values [12,13] for both In and Tl systems allows us to discard the latter values against the LPTS [11,18] results. As far as the suggestion made by Felfli *et al.* [25] is concerned, interpreting the previous thallium electron affinities as the binding energy of the first excited states of Tl^-, the present MCDHF-RCI results firmly confirm that the experimental value of 320.053(19) meV [11] should be definitely assigned to the real electron affinity. The present calculations indeed definitely exclude the possibility of a more bound state than $6s^26p^2\ ^3P_0$. Excitation ground configuration energies of In^- and their radiative lifetimes are also estimated. We confirm that In^- has three bound states $^3P_{0,1,2}$, while Tl^- only has one bound state $^3P_0$.

The isotope shift on the EAs of along In and Tl isotopes are estimated using the currently available rms nuclear radii. Although the MS contributes significantly to the indium EAs, it is already smaller than the FS contribution. For the EA(Tl), the FS largely dominate the MS that becomes almost negligible. The isotope shift between the two stable Tl^{203} and Tl^{205} isotopes is estimated to be $\mathrm{IS(EA)}^{205} - \mathrm{IS(EA)}^{205} = +0.7014$ GHz, corresponding to a "normal" isotope shift due to the gain in electron density at the nucleus accompanying the outer electron detachment from the anion.

The lifetimes estimated for the excited In^- fine structure $6s^26p^2\ ^3P_{1,2}$ levels are rather long but could be measured using a cryogenic ion storage ring. We hope that the present work will stimulate such experiments along those lines.

ACKNOWLEDGMENTS

We acknowledge support from the Belgian FWO and FNRS Excellence of Science Programme (EOS-O022818F). S.S. is a FRIA grantee of the F.R.S.-FNRS. C.Y.C. acknowledges support from the National Natural Science Foundation of China (Grants No. 12074081 and No. 11974080). K.W. expresses his gratitude for the support from the National Natural Science Foundation of China (Grant No. 11703004), and the Natural Science Foundation of Hebei Province, China (A2019201300).

[1] R. C. Bilodeau and H. K. Haugen, Phys. Rev. Lett. **85**, 534 (2000).
[2] U. Warring, M. Amoretti, C. Canali, A. Fischer, R. Heyne, J. O. Meier, C. Morhard, and A. Kellerbauer, Phys. Rev. Lett. **102**, 043001 (2009).
[3] A. Fischer, C. Canali, U. Warring, A. Kellerbauer, and S. Fritzsche, Phys. Rev. Lett. **104**, 073004 (2010).
[4] C. W. Walter, N. D. Gibson, C. M. Janczak, K. A. Starr, A. P. Snedden, R. L. Field III, and P. Andersson, Phys. Rev. A **76**, 052702 (2007).
[5] C. W. Walter *et al.*, Phys. Rev. A **84**, 032514 (2011).
[6] C. W. Walter, N. D. Gibson, D. J. Matyas, C. Crocker, K. A. Dungan, B. R. Matola, and J. Rohlén, Phys. Rev. Lett. **113**, 063001 (2014).

[7] E. Jordan, G. Cerchiari, S. Fritzsche, and A. Kellerbauer, Phys. Rev. Lett. **115**, 113001 (2015).

[8] G. Cerchiari, A. Kellerbauer, M. S. Safronova, U. I. Safronova, and P. Yzombard, Phys. Rev. Lett. **120**, 133205 (2018).

[9] R. Tang, R. Si, Z. Fei, X. Fu, Y. Lu, T. Brage, H. Liu, C. Chen, and C. Ning, Phys. Rev. Lett. **123**, 203002 (2019).

[10] R. Tang, R. Si, Z. Fei, X. Fu, Y. Lu, T. Brage, H. Liu, C. Chen, and C. Ning, Phys. Rev. A **103**, 042817 (2021).

[11] C. W. Walter, N. D. Gibson, and S. E. Spielman, Phys. Rev. A **101**, 052511 (2020).

[12] D. L. Carpenter, A. M. Covington, and J. S. Thompson, Phys. Rev. A **61**, 042501 (2000).

[13] W. W. Williams, D. L. Carpenter, A. M. Covington, J. S. Thompson, T. J. Kvale, and D. G. Seely, Phys. Rev. A **58**, 3582 (1998).

[14] M. Scheer, R. C. Bilodeau, and H. K. Haugen, Phys. Rev. Lett. **80**, 2562 (1998).

[15] M. Scheer, R. C. Bilodeau, J. Thøgersen, and H. K. Haugen, Phys. Rev. A **57**, R1493 (1998).

[16] N. D. Gibson, C. W. Walter, C. Crocker, J. Wang, W. Nakayama, J. N. Yukich, E. Eliav, and U. Kaldor, Phys. Rev. A **100**, 052512 (2019).

[17] R. Tang, X. Fu, Y. Lu, and C. Ning, J. Chem. Phys. **152**, 114303 (2020).

[18] C. W. Walter, N. D. Gibson, D. J. Carman, Y.-G. Li, and D. J. Matyas, Phys. Rev. A **82**, 032507 (2010).

[19] F. Arnau, F. Mota, and J. J. Novoa, Chem. Phys. **166**, 77 (1992).

[20] W. P. Wijesundera, Phys. Rev. A **55**, 1785 (1997).

[21] E. Eliav, Y. Ishikawa, P. Pyykkö, and U. Kaldor, Phys. Rev. A **56**, 4532 (1997).

[22] C. Guo-Xin and P. P. Ong, J. Phys. B **32**, 5351 (1999).

[23] D. Figgen *et al.*, J. Chem. Phys. **128**, 024106 (2008).

[24] J. Li, Z. Zhao, M. Andersson, X. Zhang, and C. Chen, J. Phys. B **45**, 165004 (2012).

[25] Z. Felfli, A. Z. Msezane, and D. Sokolovski, J. Phys. B **45**, 045201 (2012).

[26] B. A. Finney and K. A. Peterson, J. Chem. Phys. **151**, 024303 (2019).

[27] C. Froese Fischer, M. Godefroid, T. Brage, P. Jönsson, and G. Gaigalas, J. Phys. B **49**, 182004 (2016).

[28] P. Jönsson, G. Gaigalas, J. Bieroń, C. Froese Fischer, and I. Grant, Comput. Phys. Commun. **184**, 2197 (2013).

[29] C. Froese Fischer, G. Gaigalas, P. Jönsson, and J. Bieroń, Comput. Phys. Commun. **237**, 184 (2019).

[30] I. Grant, J. Phys. B **7**, 1458 (1974).

[31] R. D. Cowan, The Theory of Atomic Structure and Spectra, *Los Alamos Series in Basic and Applied Sciences* (University of California Press, Berkeley, 1981).

[32] J. Olsen, M. R. Godefroid, P. Jönsson, P.-Å. Malmqvist, and C. Froese Fischer, Phys. Rev. E **52**, 4499 (1995).

[33] C. Nazé, E. Gaidamauskas, G. Gaigalas, M. Godefroid, and P. Jönsson, Comput. Phys. Commun. **184**, 2187 (2013).

[34] J. Ekman *et al.*, Comput. Phys. Commun. **235**, 433 (2019).

[35] N. A. Zubova, A. V. Malyshev, I. I. Tupitsyn, V. M. Shabaev, Y. S. Kozhedub, G. Plunien, C. Brandau, and T. Stöhlker, Phys. Rev. A **93**, 052502 (2016).

[36] A. V. Malyshev, I. S. Anisimova, D. V. Mironova, V. M. Shabaev, and G. Plunien, Phys. Rev. A **100**, 012510 (2019).

[37] A. V. Malyshev, I. S. Anisimova, D. A. Glazov, M. Y. Kaygorodov, D. V. Mironova, G. Plunien, and V. M. Shabaev, Phys. Rev. A **101**, 052506 (2020).

[38] Nuclear masses are calculated by subtracting the mass of the electrons from the atomic masses [53] and adding the total binding electronic energy using the prescriptions of [54].

[39] V. M. Shabaev, Theor. Math. Phys. **63**, 588 (1985).

[40] C. W. P. Palmer, J. Phys. B **20**, 5987 (1987).

[41] V. Shabaev and A. Artemyev, J. Phys. B **27**, 1307 (1994).

[42] V. M. Shabaev, Phys. Rev. A **57**, 59 (1998).

[43] Y. S. Kozhedub, O. V. Andreev, V. M. Shabaev, I. I. Tupitsyn, C. Brandau, C. Kozhuharov, G. Plunien, and T. Stöhlker, Phys. Rev. A **77**, 032501 (2008).

[44] R. Si and C. Froese Fischer, Phys. Rev. A **98**, 052504 (2018).

[45] D. Leimbach *et al.*, Nat. Commun. **11**, 3824 (2020).

[46] I. Angeli and K. Marinova, At. Data Nucl. Data Tables **99**, 69 (2013).

[47] S. Schiffmann and M. Godefroid, J. Quant. Spectrosc. Radiat. Transf. **258**, 107332 (2021).

[48] E. Bäckström, D. Hanstorp, O. M. Hole, M. Kaminska, R. F. Nascimento, M. Blom, M. Björkhage, A. Källberg, P. Löfgren, P. Reinhed, S. Rosén, A. Simonsson, R. D. Thomas, S. Mannervik, H. T. Schmidt, and H. Cederquist, Phys. Rev. Lett. **114**, 143003 (2015).

[49] H. Zettergren, Can. J. Phys. **95**, 817 (2017).

[50] Y. Su, R. Si, K. Yao, and T. Brage, J. Phys. B **52**, 125002 (2019).

[51] T. Brage and J. Grumer, J. Phys. B **50**, 025001 (2016).

[52] A. Kramida, Yu. Ralchenko, J. Reader, and NIST ASD Team, NIST Atomic Spectra Database (ver. 5.7.1), [Online]. Available: https://physics.nist.gov/asd [2020, October 13]. National Institute of Standards and Technology, Gaithersburg, MD, 2019.

[53] G. Audi, A. Wapstra, and C. Thibault, Nucl. Phys. A **729**, 337 (2003), The 2003 NUBASE and Atomic Mass Evaluations.

[54] L. Filippin, M. Godefroid, J. Ekman, and P. Jönsson, Phys. Rev. A **93**, 062512 (2016).